LANGMUIR Article
Cite This: Langmuir XXXX, XXX, XXX−XXX
pubs.acs.org/Langmuir

Thickness-Dependent Phase Transition Drives Nanoridge-to-Mesa Instability in Micellar Freestanding Films

Yiran Zhang and Vivek Sharma*

Department of Chemical Engineering, University of Illinois at Chicago, Chicago, Illinois 60607, United States

Supporting Information

ABSTRACT: Understanding fluxes and instabilities within freestanding ultrathin films is necessary for a better understanding of, and control over, the stability and lifetime of foams and emulsions. In micellar foam films, confinement-induced layering of micelles leads to stepwise thinning or stratification that occurs by the expansion of thinner, darker domains. Often, because of a nanoridge-to-mesa instability, one or more brighter white spots or "mesas" appear at the circular moving front between thinner domains and the thicker (less dark) surrounding film. Previous studies assume that the instability and the appearance of white spots are similar to the capillarity-driven Rayleigh instability that leads to the breakup of a coherent liquid jet. Using the IDIOM (interferometry digital imaging optical microscopy) protocols we recently developed, we characterize the nanoridge-to-mesa instability with exquisite spatiotemporal resolution (thickness <1 nm, time <1 ms). The instability could be classified as a Rayleigh instability if a similar sequence of thick and thin undulations is visualized around the expanding domains. However, quantitative analysis reveals that only mesas grow in size after the instability, whereas the rest of the nanoridge preserves its shape. By analogy to the phase separation into compositionally distinct regions, we show that the spontaneous nucleation of thicker mesas in stratifying films is a phase transition driven by the oscillatory nature of the free-energy functional.

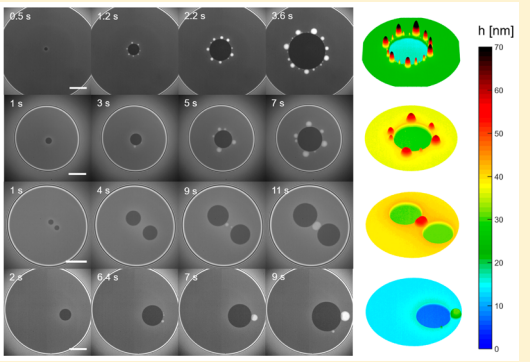

INTRODUCTION

Liquid ridges emerge near moving fronts (or contact lines) in many scientifically, aesthetically, and technologically important problems. Such ridges are susceptible to hydrodynamic instabilities that create a topographical transition to thick and thin regions forming fingers, rivulets, or drops.[1−6] For example, ridges and subsequent instabilities arise as liquid paint slides along the wall (or a canvas), liquids spread on a wetting substrate,[1−4] or during drop impact[7] and hydraulic jumps (seen in kitchen sinks[8] and rinsing flows[9]). A quantitative description of forces (including capillary, viscous, inertial, viscoelastic, and gravity) and fluxes underlying ridge instabilities is crucial for identifying the physicochemical properties that control instabilities and hence the final morphology.[1−6,10] Additional stresses due to thickness-dependent disjoining pressure contributed by intermolecular and surface forces determine the morphology, stability, and hydrodynamics of ultrathin films (thickness, h < 100 nm).[5,6,11,12] In supported ultrathin films undergoing dewetting, nanoridges[5,6,12−14] appear and expand near retreating contact lines as holes expand within the dewetting film. The characterization of hole expansion dynamics,[6] ridge shape,[14,15] and ridge instability that leaves droplets within expanding holes using techniques such as AFM[5,12] and the related theoretical advances provided critical breakthroughs for designing stable ultrathin coatings for the microelectronics industry.[5,6,12−16] Likewise, we infer that revolutionary progress in both the understanding of, and control over, the stability, morphology, and lifetime of ultrathin freestanding films of soft matter requires advances in experimental and theoretical analyses of thickness variations and instabilities, described herein. We show that a phase transition governed by an oscillatory disjoining pressure drives nanoridge-to-mesa instability in stratifying micellar freestanding films, in striking contrast to the hydrodynamic instabilities encountered in ridges near moving contact lines in supported films,[2,4,8] and to the capillary-driven Rayleigh instability assumed in previous studies on foam films.[17−19]

Ultrathin films of soft matter containing supramolecular structures such as micelles,[17,20−22] nanoparticles,[20,23−26] smectic liquid crystals,[27,28] lipid bilayers,[29,30] and polyelectrolytes[23] undergo drainage via stratification, manifested in stepwise thinning in interferometry-based measurements of average thickness.[17,20,21] In this study, we focus exclusively on stratification in micellar freestanding films formed with an aqueous solution of sodium dodecyl sulfate (SDS) above the critical micelle concentration (cmc = 8.2 mM). In addition to dispersion forces and electrostatic double-layer forces that are referred to together as the DLVO (Derjaguin−Landau−Verwey−Overbeek) forces,[31−33] the confinement-induced

Received: March 27, 2018
Revised: May 29, 2018
Published: June 4, 2018

DOI: 10.1021/acs.langmuir.8b01010
Langmuir XXXX, XXX, XXX−XXX

layering of supramolecular structures (such as micelles) gives rise to a non-DLVO, supramolecular oscillatory structural force contribution to the disjoining pressure. The supramolecular surface force term can counterbalance the capillary suction pressure between the surrounding thicker Plateau border and the plane parallel film at multiple thicknesses.[17,20,21,23] Since disjoining pressure $\Pi(h) = -(\partial G/\partial h)_{P,T,A,N_i}$ is the first derivative of the Gibbs free energy with respect to thickness,[17,21,33] thus the oscillatory contribution to free energy leads to the coexistence of different metastable thicknesses that are manifested as distinct colors or shades of gray in reflected light microscopy.[34−36] (See the Supporting Information movie.) Stratification typically proceeds via nucleation and growth of one or more thinner, darker domains that expand at the cost of the surrounding film that is thicker by a step size that equals the intermicellar distance.[17,20,21] We recently showed that nanoridges form and grow around expanding domains due to the local volume conservation,[35,36] and after the onset of the nanoridge-to-mesa instability,[34,36,37] the domain expansion kinetics changes from diffusive-like $R \propto t^{1/2}$ to constant velocity mode, i.e., $R \propto t$. A mechanistic understanding of the nanoridge-to-mesa instability and the transition in domain expansion dynamics are the two primary goals of this investigation.

Previous studies including Bergeron et al.,[17] Heinig et al.,[18] and most recently Lee et al.[19] claim that the nanoridge instability and the formation of mesas is akin to the capillarity-driven Rayleigh instability that leads to the breakup of a coherent liquid jet[10,38] or a toroidal, donut-shaped drop into a stream of droplets.[39,40] In the Rayleigh instability, thickness perturbations lead to sinusoidal undulations, creating a train of necks and swells. The capillary pressure progressively increases within the thinning neck, squeezing out fluid into the adjoining thicker swells, until a finite time singularity within the neck leads to pinch-off, creating isolated drops.[10,11,38−41] The nanoridge-to-mesa instability could be classified as a Rayleigh instability if a similar sequence of thick and thin undulations is visualized around the expanding domains. However, because of the lack of techniques that can be used for visualizing thickness variations associated with the nanoridge-to-mesa instability, such experimental evidence is entirely lacking. In this contribution, we show that the nanoridge-to-mesa instability can be analyzed using IDIOM (interferometry digital imaging optical microscopy) protocols we developed recently.[34−36,42] The IDIOM protocols allow the visualization and analysis of thickness variations in freestanding films with unprecedented detail by creating AFM-like thickness maps[36] with high spatial (thickness <1 nm, lateral ∼500 nm) and significantly higher temporal resolution (<1 ms). We recently showed that the shape and shape evolution of the nanoridge are influenced by supramolecular oscillatory surface forces that arise from the confinement-induced layering of micelles.[35] In this study, we aim to elucidate the forces and fluxes underlying the appearance of thicker mesas, which have been called lenses, bubbles, drops, and white spots in reports by other researchers.[17−19,21,37] Here we limit focus to the mesas formed at the moving contact line around expanding domains.

MATERIALS AND METHODS

Materials. The foam films are prepared with solutions of sodium dodecyl sulfate (SDS) above the critical micelle concentration (cmc). SDS (Sigma-Aldrich Co., St. Louis, MO, L6026, >99.0%) is used without further purification. The cmc of SDS is measured with maximum bubble pressure tensiometry and pendant drop tensiometry to be cmc = 8.2 mM, and the smooth transition at the cmc shows that the as-made solutions of as-received SDS are relatively free of impurities.[43] All solutions are prepared with deionized water with a resistivity of 18.2 MΩ without the addition of electrolytes.

IDIOM Protocols and Thin Film Balance. The freestanding thin films are made with micellar SDS. We use a version of the porous plate thin film apparatus[15] to control the capillary pressure, P_c, which drives the stratification of the thin film. The foam film is visualized by using a reflected light microscope assembly that consists of a precision microscope lens system (Navitar Zoom 6000) and a high-resolution, high-speed color camera (FASTCAM Mini UX100). Illumination is provided by a white LED light source (Filex P360EX, color temperature set to 5100 K). The film thickness $h(x, y, t)$ during stratification is characterized using the IDIOM protocols[34−36] that are based on the measurement of the spatiotemporal variation in interference intensity $I(x, y, t)$ and utilize the built-in photosensor array of a digital camera.[34,36] Every pixel in a color image obtained by a digital camera can be read as a composite of three intensities of red (wavelength λ = 650 nm), green (λ = 546 nm), and blue (λ = 470 nm) light, and each color channel has values in the range of 0−4095 (for a RAW image with a 12-bit depth). The IDIOM protocols rely on white light illumination and use digital filtering to obtain simultaneous intensity maps and consequently thickness measurements by using the interferometry equation[44]

$$h = \left(\frac{\lambda}{2n\pi}\right)\arcsin\left(\sqrt{\frac{\Delta}{1 + 4R(1-\Delta)/(1-R)^2}}\right) \quad (1)$$

where λ is the wavelength of light, $\Delta = (I/I_{min})/(I_{max}/I_{min})$, and $R = (n-1)^2/(n+1)^2$. Here, I is the intensity value measured in each pixel, I_{max} and I_{min} are maxima and minima intensities of interference, and n is the refractive index of the bulk solution (here n = 1.33). The image analysis is carried out in MATLAB R2015a with specially developed codes. The thicknesses measured separately from each of the three-color channels are found to be in good agreement (<1 nm difference). The IDIOM technique allows us to map the thickness of the entire film area. The thickness profiles and thickness maps included in this contribution (Figures 1−5) show the total thickness of the thin film, and the two liquid−air interfaces are assumed to have similar properties and topographical features. With the aforementioned microscope assembly, the thickness measurement reaches a spatial resolution of 0.55 μm/pixel, a thickness resolution of ∼1 nm, and a <1 ms temporal resolution.

The magnitude, oscillation frequency, and decay length of the supramolecular oscillatory surface forces can be described using the following phenomenological expression, developed and described in our previous contribution[42]

$$\Pi_{os} = \frac{(c - \text{cmc})N_A}{N_{agg}} f(\varphi) k_B T \cos\left(\frac{2\pi h}{\Delta h}\right) \exp\left[\left(\left(\frac{d}{\Delta h}\right)^3 - \frac{h}{\Delta h}\right) g(\varphi)\right] \quad (2a)$$

$$f(\varphi) = \frac{(1 + \varphi + \varphi^2 - \varphi^3)}{(1-\varphi)^3};\ g(\varphi) = \frac{\sqrt{2/3} + a_1\Delta\varphi + a_2(\Delta\varphi)^2}{(b_1/\Delta\varphi) - b_2} \quad (2b)$$

Here, the prefactor depends on temperature. The number density of the micelles is given by $\rho = (c - \text{cmc})N_A/N_{agg}$, where the aggregation number is N_{agg} and the effective volume fraction φ of the micelles is defined as $\varphi = \rho\pi d^3/6$. The expression 2a includes a compressibility factor, $f(\varphi)$, derived by Carnahan and Starling for hard spheres.[45] Parameter $\Delta\varphi = \pi/3\sqrt{2} - \varphi$ and a_1 = 0.24, a_2 = 0.63, b_1 = 0.49, and b_2 = 0.42 are based on the formulas and values determined by Kralchevsky and Denkov.[46] Here, a concentration-dependent effective size, d, is computed using $d = 2(R + \kappa^{-1})$, where the Debye length is estimated using $\kappa^2 = 8\pi l_B[\text{cmc} + \alpha(c - \text{cmc})]$. Here α is the degree of ionization and the Bjerrum length is $l_B = e^2/\varepsilon kT$ = 0.72 nm for water. The exponential term accounts for the diminishing effect of confinement with distance. Here the decay length $\Delta h/g(\varphi)$ depends

DOI: 10.1021/acs.langmuir.8b01010
Langmuir XXXX, XXX, XXX−XXX

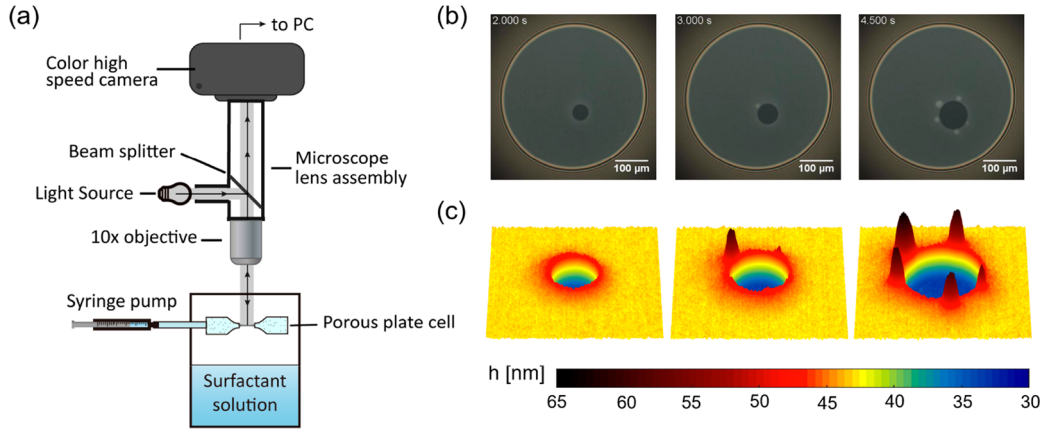

Figure 1. Schematic of thin film balance and an example of nanoridge-to-mesa instability in stratifying micellar foam films, (a) Schematic of the interferometry, digital imaging, and optical microscopy (IDIOM) setup used for quantifying thickness, $h(x, y, t)$, variations and transitions within a micellar film undergoing drainage via stratification and also for measuring the disjoining pressure isotherm. The IDIOM protocols that result in pixelwise thickness detection are based on the measurement of the spatiotemporal variation in interference intensity $I(x, y, t)$ and utilize the photosensor array of a digital camera. (b) Grayscale image of a stratifying foam film in which darker domains are thinner than the surroundings and thicker regions at the moving contact lines appear as brighter mesas. (c) Color-coded thickness maps constructed using the IDIOM method show that nanoridges that form around the expanding domain undergo an instability that leads to the appearance of thicker mesas.

on the effective volume fraction as well as the step size, and the geometric factor $g(\varphi)$ values are determined from Henderson's theory.[47] Previous studies show that the oscillatory disjoining pressure isotherm for SDS solution can be measured using a thin film balance.[21,35] For each value of imposed Laplace pressure (controlled by the changing film size or film volume), the counterbalancing disjoining pressure equilibrates in flat films for thicknesses that are quantized such that the step size is dependent on the intermicellar distance. In contrast, the thickness and the shape of nonflat (often non-equilibrium) regions such as ridges and mesas are influenced by the local curvature-dependent capillary pressure, the thickness-dependent disjoining pressure, hydrodynamic-dominated events such as coalescence, and the imposed Laplace pressure that depends on the film size and the design of the thin film balance.[35]

RESULTS AND DISCUSSION

Visualizing Diverse Morphologies Associated with Nanoridge-to-Mesa Instability. In the experiments, a single freestanding film is created in a 1 to 2 mm hole in a porous glass plate that forms part of the thin film balance (Figure 1). The plane-parallel film surrounded by a thicker meniscus emulates a foam film and its surrounding Plateau border. In conventional interferometry measurements,[17,20,21,44] an average thickness is computed using reflected light intensity obtained from a spot size of 30−60 μm. In contrast, the IDIOM protocols allow the simultaneous observation and analysis of the thickness variations accompanying domain expansion (Figure 1b,c). First, a faint halo can be detected at the moving contact line due to nanoridge formation, and later thicker, brighter white spots appear. The spatiotemporal evolution of the nanoridge-to-mesa instability can be visualized using IDIOM protocols (Figure 1c). Even though the height of the regions corresponding to white spots is in nanometers, their width is in micrometers. While the white spots have been called lenses, bubbles, or drops in reports by other researchers,[17,19,21,37] the thickness maps reveal that these white spots have a width that is nearly 1000 times larger than their height, making them topographically similar to mesas (or pancakes).[36]

The domain expansion and this topological nanoridge-to-mesa instability at the moving front around expanding domains in stratifying micellar films are investigated here for surfactant concentration ranging from 50 to 100 mM SDS in water (10 mM intervals, with at least three repeats per concentration) with no salt added. The instability evolution is investigated and described for these solutions for film thicknesses ranging from 20 to 60 nm (corresponding to the thickness transitions from h_3 to h_2, assuming that the thinnest films are described as h_0). Though we have mapped out the domain expansion dynamics and the step-size variations for an extended range of surfactant (and also monovalent salt) concentrations,[34−36,42] here we focus on a concentration range where both the domain expansion dynamics and ridge shape are clearly visualized both before and after the instability and are amenable to quantitative analysis. Likewise, though the white spots or mesas also appear in much thicker films than explored here (that is, for transitions between h_4 to h_3, for example), the likelihood of observing the nucleation of isolated domains (that is, domains that are far away from the Plateau border or other domains) and of observing the nanoridge-to-mesa instability around an expanding darker domain is higher in the later stages of stepwise thinning.

The image sequences included in Figure 2 show that the distribution of the mesas can be either periodic (Figure 2a) or aperiodic (Figure 2b). The size of the corresponding mesas, including their height and width (visualized in thickness maps constructed using IDIOM protocols as shown), varies considerably within each image sequence. Lee et al.[19] observed periodic mesas (christened as a "crown of lenses") similar to Figure 2a and cited these as evidence of a Rayleigh instability without mapping out the thickness evolution of the so-called lenses or the region in between lenses. After characterizing the stratification dynamics in scores of stratifying micellar films, we find that the periodic mesas flanking expanding domains are observed only in some instances. In most cases, mesas appear sequentially, and the shape and size of each mesa depends on its distinct instant of appearance. In such cases, the "older", larger mesas exhibit primarily radial motion because they are pushed outward along with the contact line between the expanding thinner domain and the surrounding thicker film, whereas the "younger", smaller mesas also travel along the

DOI: 10.1021/acs.langmuir.8b01010
Langmuir XXXX, XXX, XXX−XXX

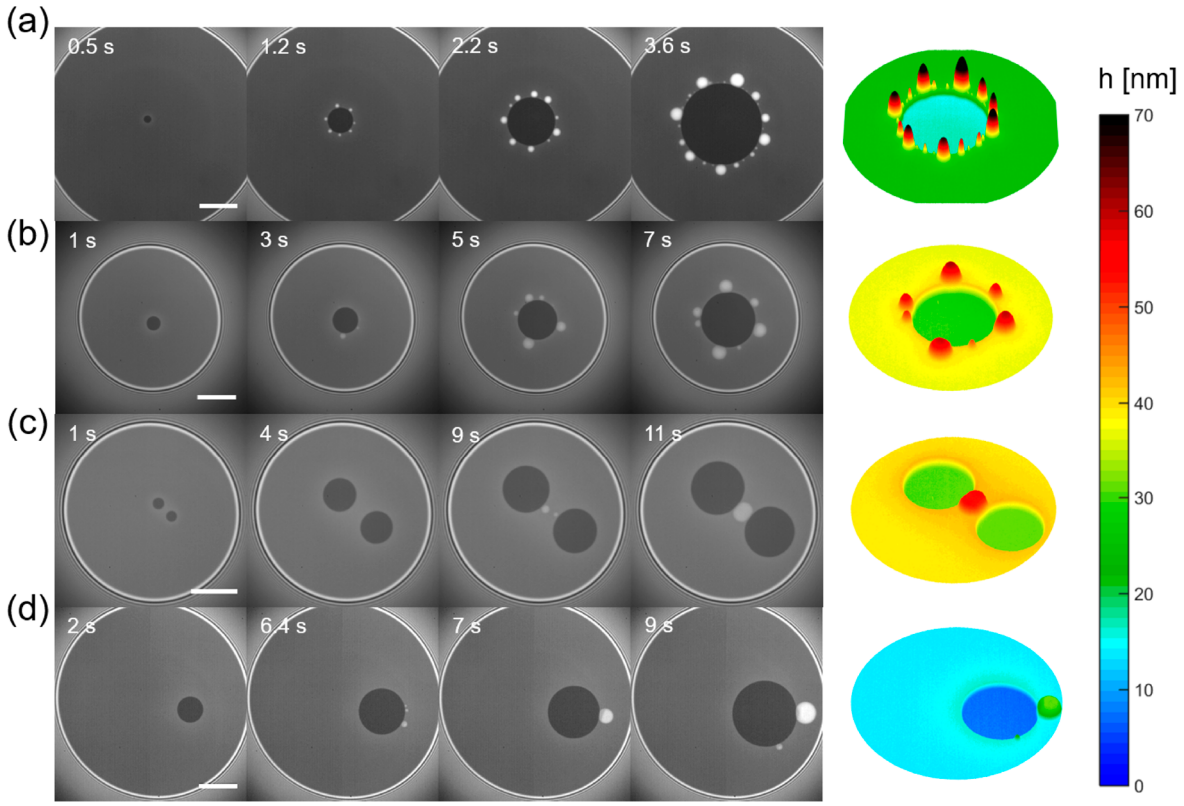

Figure 2. Visualizing diverse morphologies associated with nanoridge-to-mesa instability. Image sequences showing diverse morphologies associated with the topological instability that results in mesa formation. A color coded thickness map is constructed for the last snapshot of each sequence using the IDIOM protocols to highlight variations in the number, size, and shapes of mesas. (a) Symmetrically distributed mesas captured during the h_1 to h_0 transition in 50 mM SDS. (b) Asymmetrical growth and distribution of mesas observed during the h_2 to h_1 transition in 60 mM SDS. (c) Mesas nucleated in the isthmus between two domains, observed here from the h_3 to h_2 transition in 100 mM SDS. (d) Mesas that nucleate and grow in close proximity to the Plateau border, from the h_2 to h_1 transition in 100 mM SDS. Scale bars correspond to 100 μm.

contact line to coalesce with the larger mesas. Furthermore, in many cases, mesas are formed only locally in the region that is in the vicinity of another domain (Figure 2c) or the periphery of the film (Plateau border) (Figure 2d), indicating that the nanoridge instability is influenced by localized thickness variations, fluxes, and flows.

These observations (Figure 2b–d) are contrary to the periodicity and symmetry expected for a Rayleigh-type instability as manifested in both freestanding and supported toroidally shaped liquid rings,[39,40,48−50] where morphologies are quite sensitive to the radius of the toroid and the fluid flows creates a necklace of linked swells and necks. Freestanding toroidal rings have comparable major and minor diameters (of a few mm) and circular cross-section. In contrast, the nanoridges in the ultrathin stratifying foam films flank domains of ∼0.01 mm in diameter, our recent characterization[35] shows that the nanoridge cross section is quite unlike that of a toroid. The nanoridge in stratified films has a noncircular, highly asymmetric and relatively flat cross section, with a height of tens of nanometers and a width of micrometers.[35] (Some features were anticipated in previous theoretical studies.[17,18]) Furthermore, as the thickness-dependent disjoining pressure determines the shape and shape evolution of nanoridges,[35] it is quite likely that the mesa shape and shape evolution are dependent on $\Pi(h)$ as well. A closer look at the thickness maps in Figure 2 shows both curved-top mesas and flat-top mesas. Indeed changing $\Pi(h)$ by adding salt (or surfactant) changes the shape, size, and number of mesas formed.[42]

Spatiotemporal Evolution of the Nanoridge-to-Mesa Instability. Using thickness mapping enabled by IDIOM protocols, we can characterize the thickness variations underlying nanoridge-to-mesa instability by analyzing the film thickness profile $h(r, \theta, t)$ in and around the expanding domain. Here, r and θ denote the polar coordinates, with the origin located at the center of the thinner domain. Figure 3 shows the evolution of the nanoridge-to-mesa instability with an aperiodic distribution of mesas around the expanding domain (corresponding to the case shown in Figure 2b for 50 mM SDS solution). The contact line between the thinner domain and the nanoridge remains intact and circular (appears straight in the $r\theta$ coordinates shown in Figure 3) during the formation and growth of mesas. Furthermore, the mesas nucleate and grow on the thicker edge, away from the moving contact line, in contrast to drops that are left behind within holes during the dewetting of a liquid film on a solid substrate.[4−6,12,50] During dewetting, the contact line is significantly deformed with periodic undulations, and the thicker droplets detach from the contact line and get left behind in the thinner (dry) patch. In ridges formed in films undergoing spreading under gravitational or thermocapillary forces, thicker regions grow and advance due to lower viscous dissipation.[3−5,10] In contrast, even before mesas are manifested (at $t \approx 2.5$ s) in grayscale images of stratifying micellar films as white spots, the thickness maps show that nanoridge starts to deform by growing in both thickness and width and that local protrusions into the flat outside film can be identified (dashed

DOI: 10.1021/acs.langmuir.8b01010
Langmuir XXXX, XXX, XXX−XXX

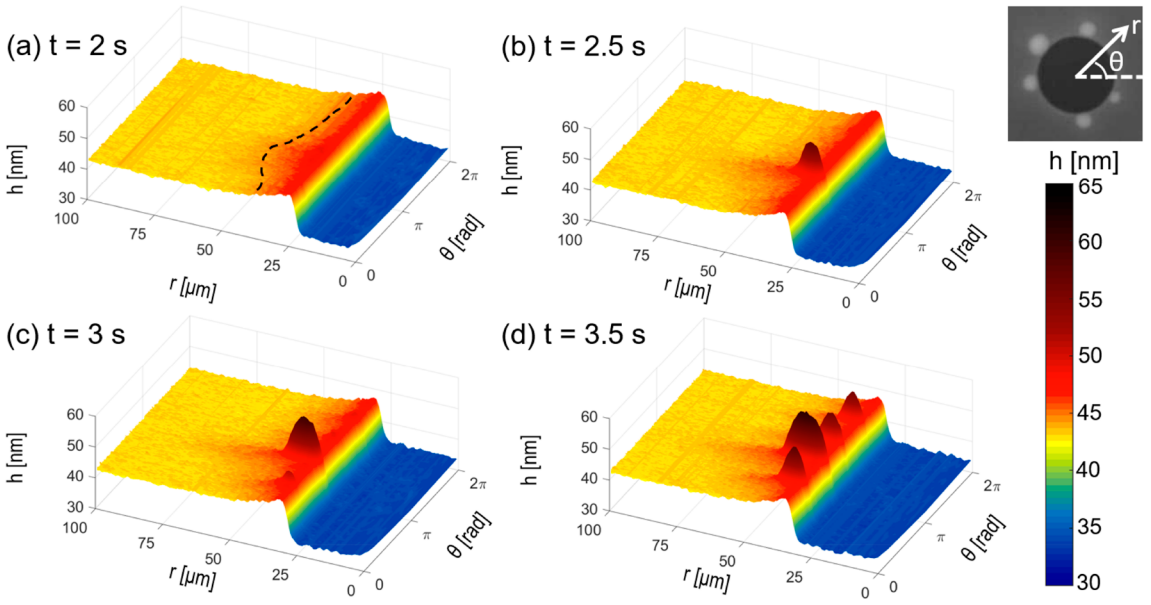

Figure 3. Spatiotemporal evolution of the nanoridge-to-mesa instability. The thickness h is plotted against distance to the domain center, r, and the rotation angle, θ. The process starts with a ridge protruding into the outside film before a thicker circular region develops adjacent to the domain contact line.

line in Figure 3a). Periodic undulation of the whole ridge is not observed, and the perturbation to nanoridge shape remains concentrated at the eventual locus of the first white spot or mesa. Finally, away from mesas, the nanoscopic ridge preserves its shape and size, as discussed in detail later. These observations indicate that the formation of mesas cannot be attributed to the breakdown of the nanoridge through Rayleigh-type instability, and the analysis of mesa growth, discussed next, rules out differential viscous growth as well.

The time evolution of the nanoridge as well as mesas is characterized in Figure 4a by plotting the maximum thickness, h_{max}, as a function of θ and t. The growth in size and thickness of mesas over time is visualized as apparent "fingers" in Figure 4a. Also visualized is the lateral movement of mesas along the contact line, leading to the later stage coalescence-assisted growth of mesas. In Figure 4b, the thickness evolution plots for two different mesas, corresponding to the regions marked in black and red dashed lines in Figure 4a, reveal three distinct growth regimes: (a) the preinstability growth characterized by the slow emergence of an axisymmetric nanoridge,[35] (b) a rapid thickness spur leading to white spot or mesa formation, and (c) the growth and coarsening of mesas. The nanoridge growth in the first regime involves thickness values (including h_{max}) that lie within a stable thickness branch (where $\partial\Pi/\partial h < 0$) of the disjoining pressure isotherm shown in Figure 4c. The thickness-dependent disjoining pressure isotherm was obtained experimentally[35] and can be described by an expression included in the Methods section based on a phenomenological model detailed elsewhere.[42] Remarkably, the second regime with the rapid height increase (due to the appearance of mesas) arises after a thickness perturbation drives the system into the unstable region of the oscillatory disjoining pressure isotherm $\Pi(h)$. In contrast, the third regime that involves a slow increase in h_{max} occurs with fluxes controlled by the next stable branch of disjoining pressure ($\partial\Pi/\partial h < 0$).

The observations of aperiodicity and the sequential appearance of mesas, their outward motion as well as their coalescence-assisted growth, and the fact that away from mesas, the ridge maintains its shape indicate that the formation of mesas cannot be attributed to the breakdown of the nanoridge through a capillary-driven Rayleigh-type instability, often cited in the stratification literature[17−19,21,37] as the mechanistic basis of the nanoridge-to-mesa instability. Thus, the quantitative characterization of the formation and evolution of mesas rules out hydrodynamic instabilities due to capillarity or viscous dissipation effects[3−6,10−13,40,49−51] and strongly suggests a thickness-dependent phase transition. The topological instabilities underlying mesa formation and the emergence of thinner, darker domains are quite analogous, even though in the latter case a metastable branch corresponding to a lower thickness gets picked. Characterizing the nanoridge shape adjacent to mesas provides further critical insights, as discussed next.

In particular, we follow the shape evolution of the nanoridge in the $0 < \theta < 0.1\pi$ region (marked with a white dashed line in Figure 4a). The total time to duration examined in Figure 5 corresponds to a period during which the domain expansion transitions from diffusive-like $R \propto t^{1/2}$ to constant velocity mode, i.e., $R \propto t$ scaling (as shown in Figure 5a). In fact, Figures 2 and 3a already suggest that the shape of the nanoridge in regions between mesas is preserved after the instability occurs. The cross-sectional shape, width, and height, as shown by the shifted thickness profiles ($h - h_\infty$ vs $r - R$) in Figure 5b evolve in regime 1, while domain expansion exhibits diffusive growth, after the onset of a topological instability, both the width, W (Figure 5c), and the maximum thickness, h_{max} (Figure 5d), attain a constant value. (Additional data set showing similar behavior for 70 mM SDS solution is included in the Supporting Information.) These observations are inconsistent with the Rayleigh-type instability. The rapid thickness variation or jump observed during the onset of the instability is also inconsistent with the viscous dissipation argument that explains why thicker fingers form and evolve faster in many cases with moving contact lines.[3,4,10]

Nanoridge-to-Mesa Instability as a Thickness-Dependent Phase Transition: Discussion. In a recent

DOI: 10.1021/acs.langmuir.8b01010
Langmuir XXXX, XXX, XXX−XXX

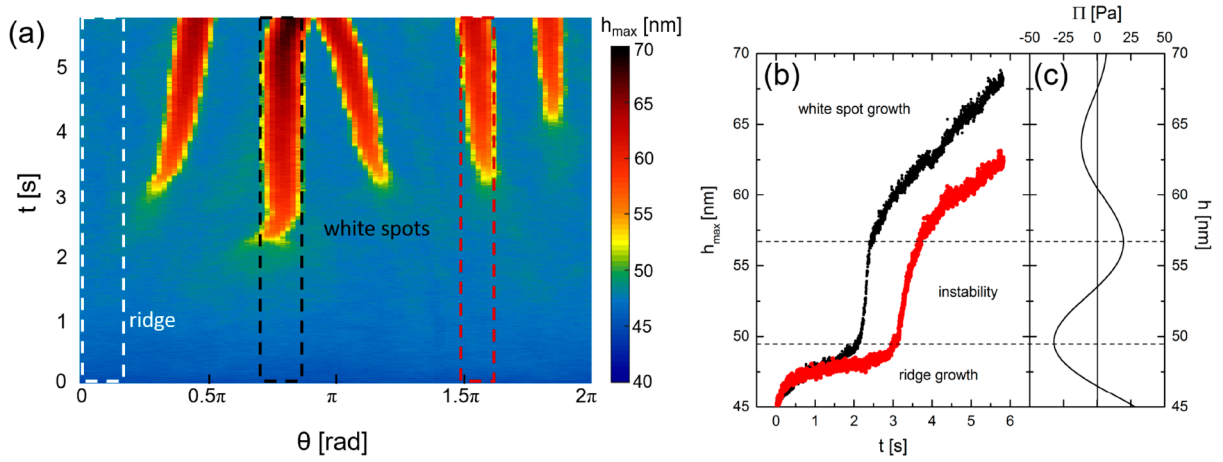

Figure 4. Thickness variation and thickness jump. (a) Spatiotemporal evolution of maximum thickness h_{max} within the nanoridge region as a function of time t and rotational angle θ is shown (using color coding). The growth of much thicker mesas over time appears as fingers in the plot, and some mesas coalesce with each other. The dotted lines mark regions where the thickness evolution of two mesas and one unperturbed ridge region is plotted in Figure 5. (b) Time dependence of maximum thickness h_{max} is shown for two mesas. (c) The disjoining pressure isotherm shown here is obtained by fitting equilibrium measurements of thickness and pressure in thin film balance with eq 2. (See the text for details.) The nanoridge-to-mesa instability involves an intermediate stage associated with a rapid increase in thickness. Slower evolution coincides with stable branches of the disjoining pressure isotherm.

contribution,[35] we showed that the complex spatiotemporal evolution of nanoridges (before the onset of instability) characterized using IDIOM protocols can be described quantitatively by using a nonlinear thin film equation model, $\partial_t h + \nabla\cdot[M\nabla P] = 0$, that explicitly accounts for the total pressure $P = \sigma K + \Pi(h)$ with two contributions: Laplace pressure arising from the local surface curvature, K, and disjoining pressure, $\Pi(h)$, contributed primarily by supramolecular oscillatory surface forces. The effective mobility term is $M = h^3/3\eta$, where η is the fluid viscosity and σ is the bulk surface tension. The nonlinear thin film equation can be considered to be a manifestation of dissipation dynamics $\partial_t\phi + \nabla\cdot[M\nabla(\delta F/\delta\phi)] = 0$ such that the evolution of conserved order parameter $\phi(r, t)$ is governed by the energy functional $F(\phi)$ (that acts as a Lyapunov parameter in this case) and thus belongs to the same class of problems as the Cahn–Hillard model for composition-based phase separation.[5,52] In the present case, height replaces composition as the order parameter, and $\delta F/\delta\phi \equiv P$.

Even though such a framework has been applied to the discussion of dewetting supported films,[6,49,51] the similarity has been left largely unexplored in the context of stratifying freestanding films. Historically, de Gennes[53] was among the first few to discuss the similarity between the nucleation and growth of holes during dewetting and the spontaneous formation and growth of black films during the thinning of (micelle-free) soap films. In both cases, the possibility of forming thicker and thinner regions is linked to the nonmonotonic, thickness-dependent disjoining pressure, and the corresponding free-energy functional $(\Pi(h) = -(\partial G/\partial h)_{P,T,A,N_i})$ has two local minima as a function of thickness. This separation of the thin film into regions of different thickness is thus quite analogous to the phase separation of (metastable) binary mixtures into compositionally distinct regions that are respectively enriched and depleted in one of the components.[52] The detailed discussion of phase separation during dewetting and the corresponding Maxwell constructions for thick and thin films can be found in several texts and reviews.[11,51,53,54] In stratified films, the disjoining pressure and the free-energy functional are oscillatory; therefore, a corresponding Maxwell construction leads to the possibility of forming thinner, darker domains and multiple coexisting thicknesses as observed as well as the spontaneous appearance of thicker regions (mesas). Though the formation of mesas or white spots in stratifying films has not been identified as a height-dependent phase transition before, the spontaneous emergence of thick and thin regions in stratified films is a consequence of a disjoining pressure (or free-energy functional) that varies with height and exhibits multiple minima and maxima (as shown in Figure 4b). A detailed exploration of the similarities and differences between hole expansion dynamics during dewetting and domain expansion dynamics during stratification is left to a future contribution. While the ridge shape evolution before and after the nanoridge-to-mesa instability can be described by nonlinear thin film equation, much like the spontaneous appearance of thinner, darker domains, the appearance of thicker white spots involves a successful thickness jump by a height comparable to the step size (Figure 4b).

For cylindrical coordinates, the nonlinear thin film equation can be written as

$$\frac{\partial h}{\partial t} + \frac{1}{r}\frac{\partial}{\partial r}\left[\frac{rh^3}{12\eta}\left(\frac{\partial \sigma K(h)}{\partial h} + \frac{\partial \Pi(h)}{\partial h}\right)\frac{\partial h}{\partial r}\right] = 0 \tag{3}$$

We recently showed that in the first regime (when $R \propto t^{1/2}$) the build-up region of the nanoridge (in contact with the thinner domain) maintains a constant contact angle and has a constant quasi-steady shape, whereas on the leeward side, the nanoridge shape is determined by a diffusive equation of the form

$$\frac{\partial h}{\partial t} + \frac{1}{r}\frac{\partial}{\partial r}\left[rD_{\text{eff}}\frac{\partial h}{\partial r}\right] = 0 \tag{4a}$$

$$D_{\text{eff}} = -\frac{h^3}{12\eta}\frac{\mathrm{d}\Pi(h)}{\mathrm{d}h} \tag{4b}$$

DOI: 10.1021/acs.langmuir.8b01010
Langmuir XXXX, XXX, XXX–XXX

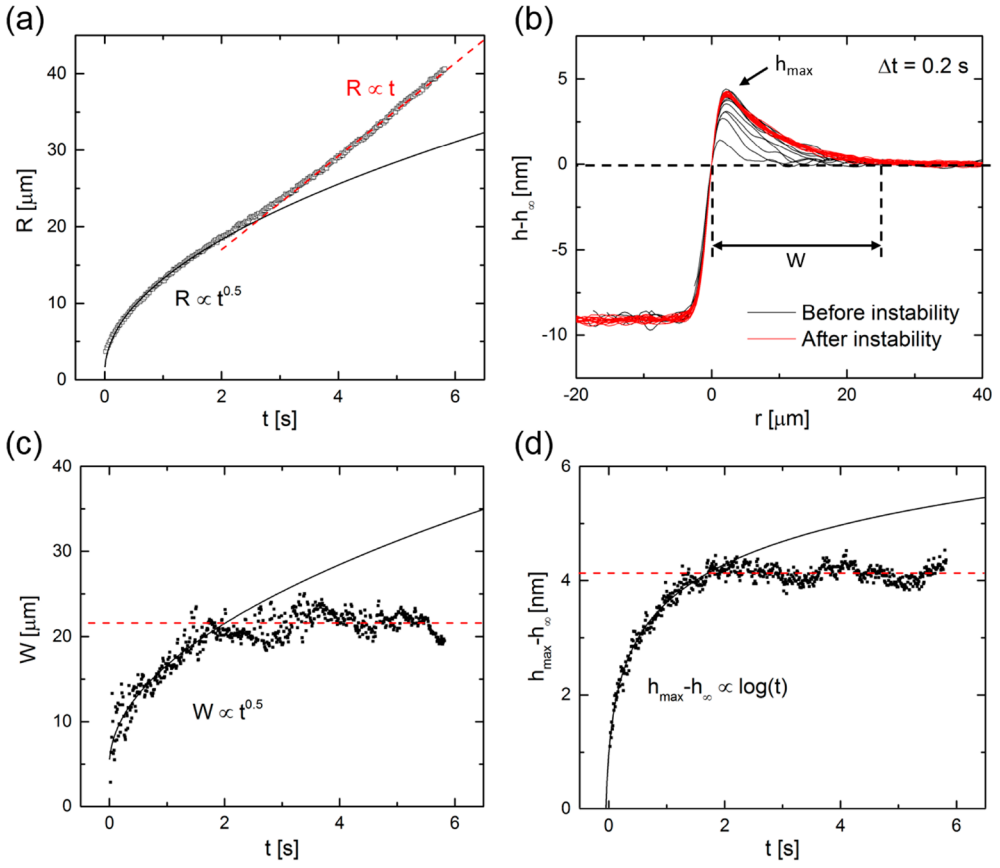

Figure 5. Domain expansion and nanoridge thickness dynamics before and after the onset of the topological instability. (a) Domain radius vs time scaling changes from $R \propto t^{0.5}$ to $R \propto t$ after the onset of instability. For the region marked with the white dotted line in Figure 4 (away from the growing mesas), the nanoridge shape and dimensions are preserved after the instability. Therefore, (b) the shifted thickness profiles of the nanoridge, $h - h_\infty$ plotted vs $r - R$, (c) nanoridge width vs time, and (d) maximum thickness of the ridge vs time show that a constant profile emerges after the onset of nanoridge-to-mesa instability.

Since the film thickness of the axisymmetric ridge before instability is comparable to the outside film thickness, i.e., $h \approx h_\infty$, D_{eff} can be approximated as a constant $D_{\text{eff}} \approx (\mathrm{d}h/\mathrm{d}r)$. Effectively, the outward flux of thickness $\Delta h(\mathrm{d}R/\mathrm{d}t)$ is controlled by the outward flux $D_{\text{eff}}(\mathrm{d}h/\mathrm{d}r)$ from the nanoridge. Equating the two fluxes shows that $\mathrm{d}R/\mathrm{d}t \propto D_{\text{eff}}/W$; that is, the domain growth expansion rate is inversely proportional to the ridge width. Before the instability, the ridge width is $W \propto t^{1/2}$, and this leads to the experimentally observed domain expansion kinetics, $R \propto D_{\text{eff}} t^{1/2}$. Thus, the rate of fluid flow out of the expanding thinner domain before the instability is effectively determined by diffusion out of the ridge region.

However, after the topological instability sets in, the ridge shape stops growing further, W becomes a constant, and the domain expansion rate $\mathrm{d}R/\mathrm{d}t \propto D_{\text{eff}}/W$ estimated using the flux balance also becomes constant. After the onset of instability, even though the diffusive growth of the ridge ceases, the liquid removed from the expanding thinner domain flows into the mesas that effectively act as sinks and grow in both size and number. The contact angle in the build-up region of the ridge (side facing the thinner, darker domain) remains constant before and after the instability for the unperturbed part of the ridge. We find that exactly the same contact angle is maintained along the contact line for the mesas of all sizes (for a given SDS concentration). Thus, the effective spreading parameter that arises at the contact line due to the difference in free energy between the flat and nonflat film remains constant before and after the instability. Though the spreading parameter provides a constant driving force, before the instability the expansion is limited by the diffusive flux out of the ridge, and since the domain expansion exhibits $R \propto D_{\text{eff}} t^{1/2}$, the contact line velocity decreases over time $V \propto t^{-1/2}$ and exhibits a critical slowing down. However, after the nanoridge-to-mesa instability, the domain expansion velocity jumps to a higher value, even though the unperturbed ridge maintains its shape as the outward and inward fluxes to the ridge are equilibrated. In this case, the domain expansion shows a constant velocity growth,[18,34,35] quite similar to the motion of capillary ridges where viscous dissipation and driving spreading parameter terms balance each other.

CONCLUSIONS

We experimentally visualize and characterize the nanoridge-to-mesa instability observed near the moving front between expanding thinner domains and their surroundings during the stratification of a micellar foam film. Using the IDIOM protocols, we show that the ridge instability is quite unlike the hydrodynamic instabilities that lead to the formation of a train of swells and necks when toroidally shaped liquid breaks up due to capillarity, drops left behind in holes during dewetting, or fingers (rivulets) formed by a difference in viscous dissipation in thick–thin regions near the contact line in spreading liquid films. The image sequences included in Figure 2 show that the distribution of the mesas can be either periodic

DOI: 10.1021/acs.langmuir.8b01010
Langmuir XXXX, XXX, XXX−XXX

(Figure 2a) or aperiodic (Figure 2b), and the size of corresponding mesas, including their height and width, varies considerably within each image sequence. We show that the contact line between the thinner domain and the nanoridge remains intact and circular during the formation and growth of mesas (Figure 3). Furthermore, the mesas nucleate and grow on the thicker edge, away from the moving contact line, in contrast to drops that are left behind within holes during the dewetting of a liquid film on a solid substrate. Likewise, we show that periodic undulation of the whole ridge is not observed, and the perturbation to the nanoridge shape remains concentrated at the eventual locus of the first mesa (Figures 4and 5). Away from the mesas, the nanoscopic ridge preserves its shape and size. Furthermore, we find that mesas often appear sequentially, and the "older", larger mesas exhibit primarily radial outward motion (pushed out with the contact line), whereas the "younger", smaller mesas also travel along the contact line to coalesce with the larger mesas. Detailed measurements of mesa size and shape evolution, statistics on their size variation, the scaling laws describing their growth before and after coalescence with each other, and the dynamics of mesas along the contact line are underway and will be presented in a future contribution.

The observations of aperiodicity and the sequential appearance of mesas, their radial and lateral motion as well as coalescence-assisted growth of mesas, the existence of flat-top mesas, and the fact that away from mesas the ridge maintains its shape indicate that the formation of mesas cannot be attributed to the breakdown of the nanoridge through a capillary-driven Rayleigh-type instability, as often presumed in the literature. Instead, we show that the supramolecular oscillatory structural force contribution to disjoining pressure plays a dominating role in driving the topological instability that leads to mesa formation and growth. As the thickness-dependent free-energy functional has an oscillatory nature, the spontaneous and relatively fast appearance of both thinner, darker domains and mesas is a manifestation of a thickness-dependent phase transition. Because of the supramolecular oscillatory contribution to the disjoining pressure, some thickness perturbations can drive the system into the unstable portion of the disjoining pressure isotherm (where $\partial\Pi/\partial h > 0$), resulting in a rapid thickness jump that leads to the almost instantanous appearance of mesas or domains (as discussed in the context of Figure 4). At the location of the mesas, three distinct regimes in thickness growth are exhibited, corresponding to a slow initial evolution (while domain grows diffusively), a rapid burst in height at the onset of instability, and the final regime in which mesas grow in width and thickness slowly and sometimes coalesce with other mesas. The nanoridge shape and size preserve its shape after the onset of instability in regions adjacent to mesas, implying that after the instability, the fluid volume from expanding domains is entirely used up in feeding the growth of mesas.

The visualization of thickness variations along the nanoridge with relatively high spatiotemporal resolution and the subsequent mechanistic understanding of the instability were made possible by the use of IDIOM protocols that we developed to examine topographical changes in freestanding films. Finally, we show that the nonlinear thin film hydrodynamics equation can be used to derive the scaling to elucidate the mechanisms underlying the transition in expansion dynamics of the thinner domain, which is consistent with experimental observations. The nonlinear thin film equation can be considered to be a manifestation of dissipation dynamics $\partial_t h + \nabla\cdot[M\nabla(\delta F/\delta h)] = 0$ such that the evolution of conserved order parameter $h(r, t)$ is governed by the energy functional $F(h)$, which belongs to the same class of problems as the Cahn−Hillard model for composition-based phase separation. Both mesa formation and domain formation are manifestations of the phase transition resulting from a thickness-dependent free energy. Remarkably, the formation of nanoridges and the subsequent nanoridge-to-mesa instability are not reported near moving fronts in stratified films formed by the layering of small molecules[55] or supramolecular structures in lipids and smectic liquid crystal films.[27] Likewise, the diffusive domain expansion regime is also unique to micellar foam films. Nevertheless, the study of the nanoridge-to-mesa instability provides critical insights into how non-DLVO, structural forces influence the dynamics, stability, and lifetime of ultrathin freestanding films and therefore of foams and other multicomponent colloidal systems.

■ ASSOCIATED CONTENT

Supporting Information

The Supporting Information is available free of charge on the ACS Publications website at DOI: 10.1021/acs.langmuir.8b01010.

Thickness evolution during domain expansion in a stratifying micellar film (PDF)

Coexistence of different metastable thicknesses that are manifest as distinct colors or shades of gray in reflected light microscopy (AVI)

■ AUTHOR INFORMATION

Corresponding Author

*E-mail: viveks@uic.edu.

ORCID

Vivek Sharma: 0000-0003-1152-1285

Notes

The authors declare no competing financial interest.

■ ACKNOWLEDGMENTS

V.S. acknowledges funding support from the College of Engineering and the Department of Chemical Engineering at the University of Illinois at Chicago. We acknowledge discussions with the followig ODES laboratory students: Subinuer Yilixiati on the supramolecular oscillatory surface force contributions and Jelena Dinic and Prerana Rathore on ridge shape evolution. We thank several students from the ODES laboratory (Carina Martinez, Chrystian Ochoa, and Subinuer) and Prof. Cynthia Jameson for a close reading of the manuscript draft.

■ REFERENCES

(1) Joanny, J. F.; de Gennes, P. G. Upward Creep of a Wetting Fluid: A Scaling Analysis. *J. Phys. (Paris)* **1986**, *47*, 121−127.

(2) Cazabat, A. M.; Heslot, F.; Troian, S. M.; Carles, P. Fingering Instability of Thin Spreading Films Driven by Temperature Gradients. *Nature* **1990**, *346*, 824−826.

(3) Oron, A.; Davis, S. H.; Bankoff, S. G. Long-Scale Evolution of Thin Liquid Films. *Rev. Mod. Phys.* **1997**, *69*, 931.

(4) Craster, R. V.; Matar, O. K. Dynamics and Stability of Thin Liquid Films. *Rev. Mod. Phys.* **2009**, *81*, 1131−1198.

(5) Kalliadasis, S.; Thiele, U. *Thin Films of Soft Matter*; SpringerWien: New York, 2007.

DOI: 10.1021/acs.langmuir.8b01010
Langmuir XXXX, XXX, XXX−XXX

(6) Blossey, R. *Thin Liquid Films: Dewetting and Polymer Flow*; Springer: 2012.
(7) Yarin, A. L. Drop Impact Dynamics: Splashing, Spreading, Receding, Bouncing. *Annu. Rev. Fluid Mech.* **2006**, *38*, 159−192.
(8) Bush, J. W. M.; Aristoff, J. M.; Hosoi, A. E. An Experimental Investigation of the Stability of the Circular Hydraulic Jump. *J. Fluid Mech.* **2006**, *558*, 33−52.
(9) Walker, T. W.; Hsu, T. T.; Frank, C. W.; Fuller, G. G. Role of Shear-Thinning on the Dynamics of Rinsing Flow by an Impinging Jet. Phys. *Phys. Fluids* **2012**, *24*, 093102.
(10) Gallaire, F.; Brun, P.-T. Fluid Dynamic Instabilities: Theory and Application to Pattern Forming in Complex Media. *Philos. Trans. R. Soc., A* **2017**, *375*, 20160155.
(11) de Gennes, P. G.; Brochard-Wyart, F.; Quéré, D. *Capillarity and Wetting Phenomena: Drops, Bubbles, Pearls, Waves*; Springer: 2004.
(12) Mukherjee, R.; Sharma, A. Instability, Self-Organization and Pattern Formation in Thin Soft Films. *Soft Matter* **2015**, *11*, 8717−8740.
(13) Becker, J.; Grün, G.; Seemann, R.; Mantz, H.; Jacobs, K.; Mecke, K. R.; Blossey, R. Complex Dewetting Scenarios Captured by Thin-Film Models. *Nat. Mater.* **2003**, *2*, 59−63.
(14) Seemann, R.; Herminghaus, S.; Jacobs, K. Shape of a Liquid Front Upon Dewetting. *Phys. Rev. Lett.* **2001**, *87*, 196101.
(15) Seemann, R.; Herminghaus, S.; Neto, C.; Schlagowski, S.; Podzimek, D.; Konrad, R.; Mantz, H.; Jacobs, K. Dynamics and Structure Formation in Thin Polymer Melt Films. *J. Phys.: Condens. Matter* **2005**, *17*, S267.
(16) Seemann, R.; Herminghaus, S.; Jacobs, K. Dewetting Patterns and Molecular Forces: A Reconciliation. *Phys. Rev. Lett.* **2001**, *86*, 5534.
(17) Bergeron, V.; Jimenez-Laguna, A. I.; Radke, C. J. Hole Formation and Sheeting in the Drainage of Thin Liquid Films. *Langmuir* **1992**, *8*, 3027−3032.
(18) Heinig, P.; Beltran, C. M.; Langevin, D. Domain Growth Dynamics and Local Viscosity in Stratifying Foam Films. *Phys. Rev. E* **2006**, *73*, 051607.
(19) Lee, J.; Nikolov, A.; Wasan, D. Stepwise Dynamics of an Anionic Micellar Film−Formation of Crown Lenses. *J. Colloid Interface Sci.* **2017**, *496*, 60−65.
(20) Nikolov, A. D.; Wasan, D. T.; Kralchevsky, P. A.; Ivanov, I. B. In *Ordered Structures in Thinning Micellar Foam and Latex Films, Ordering and Organisation in Ionic Solutions*; Sogami, N. I. a. I., Ed.; World Scientific: Singapore, 1988; pp 302−414.
(21) Bergeron, V.; Radke, C. J. Equilibrium Measurements of Oscillatory Disjoining Pressures in Aqueous Foam Films. *Langmuir* **1992**, *8*, 3020−3026.
(22) Langevin, D.; Sonin, A. A. Thinning of Soap Films. *Adv. Colloid Interface Sci.* **1994**, *51*, 1−27.
(23) von Klitzing, R.; Thormann, E.; Nylander, T.; Langevin, D.; Stubenrauch, C. Confinement of Linear Polymers, Surfactants, and Particles between Interfaces. *Adv. Colloid Interface Sci.* **2010**, *155*, 19−31.
(24) Wasan, D.; Nikolov, A. Thin Liquid Films Containing Micelles or Nanoparticles. *Curr. Opin. Colloid Interface Sci.* **2008**, *13*, 128−133.
(25) Zeng, Y.; Schön, S.; Carl, A.; von Klitzing, R. Colloidal Particles in Thin Liquid Films. *Colloid Process Engineering*; Springer: 2015; pp 3−19.
(26) Sethumadhavan, G. N.; Nikolov, A. D.; Wasan, D. T. Film Stratification in the Presence of Colloidal Particles. *Langmuir* **2001**, *17*, 2059−2062.
(27) Oswald, P.; Pieranski, P. *Smectic and Columnar Liquid Crystals: Concepts and Physical Properties Illustrated by Experiments*; CRC Press: 2005.
(28) Pieranski, P.; Beliard, L.; Tournellec, J.-P.; Leoncini, X.; Furtlehner, C.; Dumoulin, H.; Riou, E.; Jouvin, B.; Fénerol, J.-P.; Palaric, P. Physics of Smectic Membranes. *Phys. A* **1993**, *194*, 364−389.
(29) Exerova, D.; Lalchev, Z. Bilayer and Multilayer Foam Films: Model for Study of the Alveolar Surface and Stability. *Langmuir* **1986**, *2*, 668−671.
(30) Beltramo, P. J.; Vermant, J. Simple Optical Imaging of Nanoscale Features in Free-Standing Films. *ACS Omega* **2016**, *1*, 363−370.
(31) Fennell Evans, D.; Wennerström, H. *The Colloidal Domain: Where Physics, Chemistry, Biology, and Technology Meet*, 2nd ed.; Wiley-VCH: New York, 1999.
(32) Israelachvili, J. N. *Intermolecular and Surface Forces*, 3rd ed.; Academic Press: 2011.
(33) Derjaguin, B. V.; Churaev, N. V.; Muller, V. M. *Surface Forces*; Springer: New York, 1987.
(34) Zhang, Y.; Sharma, V. Domain Expansion Dynamics in Stratifying Foam Films: Experiments. *Soft Matter* **2015**, *11*, 4408−4417.
(35) Zhang, Y.; Sharma, V. Nanoridge Formation and Dynamics of Stratification in Micellar Freestanding Films. *Langmuir* **2018**, *34*, 1208−1217.
(36) Zhang, Y.; Yilixiati, S.; Pearsall, C.; Sharma, V. Nanoscopic Terraces, Mesas, and Ridges in Freely Standing Thin Films Sculpted by Supramolecular Oscillatory Surface Forces. *ACS Nano* **2016**, *10*, 4678−4683.
(37) Sonin, A.; Langevin, D. Stratification Dynamics of Thin Films Made from Aqueous Micellar Solutions. *EPL* **1993**, *22*, 271.
(38) Eggers, J. Nonlinear Dynamics and Breakup of Free-Surface Flows. *Rev. Mod. Phys.* **1997**, *69*, 865−929.
(39) Pairam, E.; Fernández-Nieves, A. Generation and Stability of Toroidal Droplets in a Viscous Liquid. *Phys. Rev. Lett.* **2009**, *102*, 234501.
(40) Fragkopoulos, A. A.; Pairam, E.; Berger, E.; Fernandez-Nieves, A. Toroidal Droplets: Growth Rates, Dispersion Relations, and Behavior in the Thick-Torus Limit. *Langmuir* **2018**, *34*, 1218−1224.
(41) Sharma, V.; Haward, S. J.; Serdy, J.; Keshavarz, B.; Soderlund, A.; Threlfall-Holmes, P.; McKinley, G. H. The Rheology of Aqueous Solutions of Ethyl Hydroxy-Ethyl Cellulose (EHEC) and Its Hydrophobically Modified Analogue (hmEHEC): Extensional Flow Response in Capillary Break-up, Jetting (ROJER) and in a Cross-Slot Extensional Rheometer. *Soft Matter* **2015**, *11*, 3251−3270.
(42) Yilixiati, S.; Rafiq, R.; Zhang, Y.; Sharma, V. Influence of Salt on Supramolecular Oscillatory Structural Forces and Stratification in Micellar Freestanding Films. *ACS Nano* **2018**, *12*, 1050.
(43) Mysels, K. J. Surface Tension of Solutions of Pure Sodium Dodecyl Sulfate. *Langmuir* **1986**, *2*, 423−428.
(44) Sheludko, A. Thin Liquid Films. *Adv. Colloid Interface Sci.* **1967**, *1*, 391−464.
(45) Carnahan, N. F.; Starling, K. E. Equation of State for Nonattracting Rigid Spheres. *J. Chem. Phys.* **1969**, *51*, 635−636.
(46) Kralchevsky, P. A.; Denkov, N. D. Analytical Expression for the Oscillatory Structural Surface Force. *Chem. Phys. Lett.* **1995**, *240*, 385−392.
(47) Henderson, D. An Explicit Expression for the Solvent Contribution to the Force between Colloidal Particles Using a Hard Sphere Model. *J. Colloid Interface Sci.* **1988**, *121*, 486−490.
(48) Zhang, Z.; Hilton, G. C.; Yang, R.; Ding, Y. Capillary Rupture of Suspended Polymer Concentric Rings. *Soft Matter* **2015**, *11*, 7264−7269.
(49) Sharma, A.; Reiter, G. Instability of Thin Polymer Films on Coated Substrates: Rupture, Dewetting, and Drop Formation. *J. Colloid Interface Sci.* **1996**, *178*, 383−399.
(50) Brochard-Wyart, F.; Redon, C. Dynamics of Liquid Rim Instabilities. *Langmuir* **1992**, *8*, 2324−2329.
(51) Thiele, U. Note on Thin Film Equations for Solutions and Suspensions. *Eur. Phys. J.: Spec. Top.* **2011**, *197*, 213−220.
(52) Vrij, A. Possible Mechanism for Spontaneous Rupture of Thin Free Liquid Films. *Discuss. Faraday Soc.* **1966**, *42*, 23−33.
(53) de Gennes, P. G. Dynamics of Drying and Film-Thinning. *Physics of Amphiphilic Layers*; Springer: 1987; pp 64−71.

DOI: 10.1021/acs.langmuir.8b01010
Langmuir XXXX, XXX, XXX−XXX

(54) Starov, V. M.; Velarde, M. G.; Radke, C. J. *Wetting and Spreading Dynamics*; CRC Press: New York, 2007.
(55) Heslot, F.; Fraysse, N.; Cazabat, A. M. Molecular Layering in the Spreading of Wetting Liquid Drops. *Nature* **1989**, *338*, 640−642.

DOI: 10.1021/acs.langmuir.8b01010
Langmuir XXXX, XXX, XXX−XXX